European Journal of Radiology xxx (2014) xxx–xxx

European Journal of Radiology

journal homepage: www.elsevier.com/locate/ejrad

Alveolar echinococcosis of the liver: Diffusion-weighted MRI findings and potential role in lesion characterisation☆

Fabio Becce[a], Anastasia Pomoni[a], Emilie Uldry[b], Nermin Halkic[b], Pu Yan[c], Reto Meuli[a], Sabine Schmidt[a,*]

[a] Department of Diagnostic and Interventional Radiology, Lausanne University Hospital, Rue du Bugnon 46, 1011 Lausanne, Switzerland
[b] Department of Visceral Surgery, Lausanne University Hospital, Rue du Bugnon 46, 1011 Lausanne, Switzerland
[c] University Institute of Pathology, Lausanne University Hospital, Rue du Bugnon 25, 1011 Lausanne, Switzerland

ARTICLE INFO

Article history:
Received 31 October 2013
Accepted 27 December 2013

Keywords:
Alveolar echinococcosis
Parasites
Liver
Magnetic resonance imaging (MRI)
Diffusion-weighted MRI (DWI)
Apparent diffusion coefficient (ADC)

ABSTRACT

Purpose: To report the diffusion-weighted MRI findings in alveolar echinococcosis (AE) of the liver and evaluate the potential role of apparent diffusion coefficients (ADCs) in the characterisation of lesions.
Materials and methods: We retrospectively included 22 patients with 63 AE liver lesions (≥1 cm), examined with 3-T liver MRI, including a free-breathing diffusion-weighted single-shot echo-planar imaging sequence (*b*-values = 50, 300 and 600 s/mm^2). Two radiologists jointly assessed the following lesion features: size, location, presence of cystic and/or solid components (according to Kodama's classification system), relative contrast enhancement, and calcifications (on CT). The ADC_{total}, ADC_{min} and ADC_{max} were measured in each lesion and the surrounding liver parenchyma.
Results: Three type 1, 19 type 2, 17 type 3, three type 4 and 21 type 5 lesions were identified. The mean (±SD) ADC_{total}, ADC_{min} and ADC_{max} for all lesions were 1.73 ± 0.50, 0.76 ± 0.38 and $2.63 \pm 0.76 \times 10^{-3}$ mm^2/s, respectively. The mean ADC_{total} for type 1, type 2, type 3, type 4 and type 5 lesions were 1.97 ± 1.01, 1.76 ± 0.53, 1.73 ± 0.41, 1.15 ± 0.42 and $1.76 \pm 0.44 \times 10^{-3}$ mm^2/s, respectively. No significant differences were found between the five lesion types, except for type 4 ($p = 0.0363$). There was a significant correlation between the presence of a solid component and low ADC_{min} ($r = 0.39$, $p = 0.0016$), whereas an inverse correlation was found between the relative contrast enhancement and ADC_{total} ($r = -0.34$, $p = 0.0072$).
Conclusion: The ADCs of AE lesions are relatively low compared to other cystic liver lesions, which may help in the differential diagnosis. Although ADCs are of little use to distinguish between the five lesion types, their low value reflects the underlying solid component.

1. Introduction

Alveolar echinococcosis (AE) is a rare zoonosis caused by the larval stage of the tapeworm *Echinococcus multilocularis* [1]. This chronic and life-threatening disease is confined to the northern hemisphere, typically found in endemic regions of western and central Europe, as well as central and eastern Asia, particularly China [1–3]. Mainly transmitted by the fox, which disseminates parasite eggs through the faeces, the metacestodes of *E. multilocularis* initially grow in the liver of infected humans by external vesiculation [3,4]. The uni- or multilocular cysts are surrounded by an intense fibroinflammatory host response, and AE lesions eventually invade the portal and/or hepatic veins, as well as intrahepatic bile ducts. They can also extend to extrahepatic sites, such as the spleen and lungs [4,5].

Imaging plays an important role in the diagnosis of AE, since the latter is based on the results of cross-sectional imaging, immunoserology, histopathology and/or detection of species-specific deoxyribonucleic acid on metacestode samples [3,4]. Ultrasonography (US) is generally the first-line examination and usually complemented by computed tomography (CT) and/or magnetic resonance imaging (MRI) [4–7]. While the typical calcification pattern is best depicted on CT, MRI demonstrates more accurately the characteristic multivesicular appearance of AE lesions, necrotic areas and invasion of vascular, biliary and/or extrahepatic structures [4–7]. To systematise the various imaging features and gain insight into the disease pathophysiology, Kodama et al. proposed a MRI classification system for AE liver lesions [8]. They were

* Corresponding author. Tel.: +41 79 556 06 44; fax: +41 21 314 44 43.
E-mail address: sabine.schmidt@chuv.ch (S. Schmidt).

0720-048X/$ – see front matter © 2014 The Authors. Published by Elsevier Ireland Ltd. All rights reserved.
http://dx.doi.org/10.1016/j.ejrad.2013.12.025

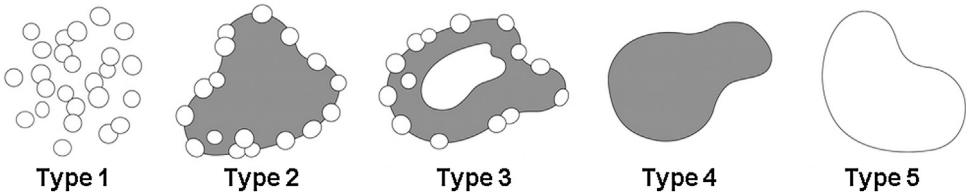

Fig. 1. Illustrative diagram of Kodama's classification system for AE liver lesions (adapted from [8]). Type 1 and type 2 lesions consist of multiple small round cysts (white) without (type 1) or with (type 2) a solid component (grey). Type 3 lesions are composed of multiple small round cysts with a solid component surrounding one or more large and/or irregular cyst(s). Type 4 lesions consist of a solid component without cyst, whereas type 5 a large and/or irregular cyst without solid component.

categorised into five types, according to the presence of cystic and/or solid components, the pattern of the cystic component, and the distribution pattern of those two components in the lesions (Fig. 1). However, due to their ill-defined contours and infiltrative growth pattern, AE lesions may mimic primary or secondary liver neoplasms [4,5].

Diffusion-weighted MRI (DWI) is based on the random microscopic motion of water protons and enables qualitative and quantitative assessment of tissue diffusivity by means of the apparent diffusion coefficient (ADC) [9,10]. DWI is increasingly used in abdominal MRI, particularly to detect and characterise focal liver lesions (FLLs) [10–12]. A few recent studies have demonstrated its value in the evaluation of cystic echinococcosis of the liver (caused by *Echinococcus granulosus*) [13–16]. To our knowledge, no study investigating the value of DWI in liver AE has been performed so far.

Thus, the purpose of our study was to report the DWI findings in liver AE and evaluate the potential role of ADCs in the characterisation of lesions.

2. Materials and methods

2.1. Patients

By searching in the radiological and surgical databases (search terms: alveolar echinococcosis, liver, MRI; search period: January 2008 to May 2013) of Lausanne University Hospital, a total of 29 patients examined with liver MRI for suspected AE were firstly identified. Five patients had to be excluded because the initial MRI scan did not include diffusion-weighted sequences, whereas two additional patients had no preoperative MRI. Hence, the final study population consisted of 22 patients (14 women, 8 men; mean age 63 years, range 22–82) with liver AE, whose diagnosis was confirmed by immunoserology ($n = 21$), surgery with subsequent pathological analysis (gross and microscopic examinations, $n = 15$) and/or suggestive cross-sectional imaging findings on initial and follow-up examinations. Three patients had an underlying liver disease (one fibrosis, one cirrhosis and one haemosiderosis) confirmed by intraoperative biopsy of the surrounding liver parenchyma, whereas all others ($n = 19$) had a normal liver on imaging and/or intraoperative biopsy ($n = 12$). Besides, 21 patients had a previous CT scan available for review (18 performed within one month of the MRI), while 12 had a previous US.

This single-centre retrospective study was approved by the institutional ethics committee, with waiver of patient informed consent. It was carried out in accordance with *The Code of Ethics of the World Medical Association* (*Declaration of Helsinki*) for experiments involving humans.

2.2. MRI protocol

All MRI scans were performed on one of two 3-T systems (Magnetom Trio or Verio; Siemens Healthcare, Erlangen, Germany) with maximum gradient strengths of 45 mT/m and slew rates of 200 T/m/s, using two 6-channel phased-array body coils anteriorly and two 3-channel spine clusters posteriorly. We used our routine liver MRI protocol but only the following axial pulse sequences were reviewed for the study purpose: breath-hold T2-weighted half-Fourier acquisition single-shot turbo spin-echo (HASTE; repetition time (TR)/echo time (TE), 1200/89 ms; echo-train length (ETL), 256; number of excitations (NEX), 1; matrix size, 320 × 240; section thickness/gap, 3/0.3 mm); respiration-triggered fat-suppressed (FS) T2-weighted turbo spin-echo (TR/TE, 5300/88 ms (dependent on the respiratory rate); ETL, 15; NEX, 3; matrix size, 448 × 336; section thickness/gap, 5/1.5 mm); free-breathing FS DW single-shot echo-planar imaging (DW-SS-EPI; TR/TE, 6500/66 ms; ETL, 1; receiver bandwidth, 1698 Hz/pixel; NEX, 3; matrix size, 168 × 126; section thickness/gap, 6/1.8 mm); and breath-hold dynamic (arterial, portal venous and equilibrium phases) gadolinium-enhanced (Dotarem, 0.2 ml/kg (0.1 mmol/kg) of body weight, followed by normal saline flush; Guerbet, Villepinte, France) FS three-dimensional T1-weighted gradient-echo (volume interpolated breath-hold examination, VIBE; TR/TE, 4.6/1.7 ms; ETL, 1; flip angle, 9°; NEX, 1; matrix size, 448 × 336; section thickness/gap, 4/0.8 mm).

All those sequences were performed using the generalised autocalibrating partially parallel acquisition (GRAPPA) technique with an acceleration factor of 2. The DWI-SS-EPI sequence was acquired before intravenous administration of contrast medium, with the patient breathing freely but shallowly. Fat suppression was achieved using the spectrally adiabatic inversion recovery (SPAIR) technique. The diffusion gradients were applied in three orthogonal directions (section, phase and frequency encoding directions), with increasing *b*-values of 50, 300 and 600 s/mm^2. These *b*-values were selected for the same reasons as described elsewhere (higher contrast-to-noise ratio, while limiting pseudodiffusion/perfusion effects [11,17]). Trace images were synthesised for each *b*-value and the corresponding ADC map automatically generated from all diffusion weightings and directions, with a noise level set to 10. The voxel size of the DWI-SS-EPI sequence was 2.3 mm × 2.3 mm × 6.0 mm and acquisition time approximately 7 min.

2.3. Image analysis

All MRI and CT examinations were reviewed by two radiologists (with 8 and 3 years of experience in abdominal MRI, respectively) on a picture archiving and communication system (PACS) workstation (Carestream Vue, version 11.3; Carestream Health, Rochester, NY, USA), reaching consensus agreement.

For each patient, the following items were assessed:

(a) The number of AE liver lesions, with their maximum diameter (measured on diffusion-weighted MR images, *b*-value = 50 s/mm^2) and location according to Couinaud's segmental anatomy. Although Holzapfel et al. reported that DWI was also helpful to characterise small (≤1 cm) FLLs [17], we considered only AE lesions with a maximum diameter ≥1 cm due

to the limited spatial resolution of ADC maps with the inherent risk of measurement errors. Eight lesions were therefore excluded and a total of 63 AE liver lesions finally included in the analysis.

(b) The presence of invasion of the portal and/or hepatic veins, and/or intrahepatic bile ducts, as well as lobar atrophy or focal capsular retraction.

(c) The mean ADC of the surrounding liver parenchyma. This was executed by placing a circular region of interest (ROI) of approximately 1 cm^2 in segment VI (whenever possible, $n = 20$) or segment V ($n = 2$), directly on the ADC map. Three consecutive measurements were performed and the median values recorded.

For each AE lesion, the following features were subsequently assessed:

(a) The presence of cystic (including distinction between small and large (≥2 cm) cysts) and/or solid components, with categorisation according to Kodama's classification system [8]. The solid component of the lesions was defined as any portion that was not as hyperintense as the cerebrospinal fluid on T2-weighted MR images [8,18].

(b) The relative contrast enhancement, which was calculated as follows on T1-weighted VIBE MR images: (mean $SI_{portal\ venous}$ − mean $SI_{unenhanced}$)/mean $SI_{unenhanced}$, where $SI_{portal\ venous}$ and $SI_{unenhanced}$ are the mean signal intensities measured in free-hand ROIs drawn in the lesion (and encompassing as much of the lesion as possible) on portal venous and unenhanced phases, respectively. The measurements were repeated three times consecutively and the median values recorded.

(c) The presence of clustered microcalcifications and/or large calcification foci on axial CT images.

(d) The mean ADC (ADC_{total}) of the lesion, with the minimum (ADC_{min}) and maximum (ADC_{max}) values. Firstly, the readers agreed on the diffusion-weighted MR image (*b*-value = 50 s/mm^2) that best depicted the lesion. Then, they drew a free-hand ROI in the lesion (again paying attention to encompass as much of the lesion as possible), which was subsequently copied and pasted on the corresponding ADC map. Again, the measurements were repeated three times consecutively and the median values of ADC_{total}, ADC_{min} and ADC_{max} recorded.

2.4. Statistical analysis

The data were processed using two statistical software packages (JMP, version 10.0; SAS, Cary, NC, USA; and IBM SPSS Statistics, version 21.0; IBM, Armonk, NY, USA). One-way analysis of variance (ANOVA) and Chi-squared tests were used to compare the continuous and categorical variables between the five lesion types, respectively. Furthermore, pairwise comparisons were performed when statistical significance was reached. Pearson's correlation coefficients (r) were used to assess potential associations between the various MRI features and ADCs. *P*-values <0.05 were considered to be statistically significant.

3. Results

The mean (± standard deviation, SD) number of AE liver lesions per patient was 2.9 ± 2.3 (range, 1–9). The average lesion size (maximum diameter) was 3.4 ± 3.0 cm (range, 1.0–14.2 cm). The lesion distribution was as follows: segment I ($n = 7$, 11%), segment II ($n = 9$, 14%), segment III ($n = 2$, 3%), segment IVa ($n = 4$, 6%), segment IVb ($n = 3$, 5%), segment V ($n = 5$, 8%), segment VI ($n = 6$, 10%), segment VII ($n = 13$, 21%) and segment VIII ($n = 14$, 22%). Thirty-eight (60%) lesions were located in the right lobe. Vascular invasion was found in 18 (82%) patients, whereas 15 (68%) had an invasion of intrahepatic bile ducts. No patient had lobar atrophy or focal capsular retraction. Fifty-five (87%) lesions were at least faintly enhanced after contrast medium administration, whereas 8 (13%) showed no enhancement. The mean relative contrast enhancement was 0.29 ± 0.22 (range, 0–1.09). Thirty-five (56%) lesions were at least partly calcified on CT. Clustered microcalcifications were found in 34 (54%) lesions, large calcification foci in 6 (10%) and both patterns in 4 (6%) lesions.

According to Kodama's classification system, we found 3 (5%) type 1, 19 (30%) type 2 (Fig. 2), 17 (27%) type 3 (Fig. 3), 3 (5%) type 4 and 21 (33%) type 5 lesions. The MRI (including DWI) findings as a function of the AE lesion type are reported in Table 1. We noted statistically significant differences in size between the five lesion types ($p < 0.0001$). Type 3 lesions were the largest (6.1 ± 2.2 cm), whereas type 4 and 5 the smallest (1.3 ± 0.1 and 1.3 ± 0.3 cm, respectively). The lesion distribution in the liver and relative contrast enhancement did not differ significantly between the five lesion types ($p = 0.4951$ and $p = 0.5744$, respectively). There were however significant differences in prevalence of calcifications ($p = 0.0002$). Type 3 lesions were most frequently calcified ($n = 15$, 88%), whereas type 5 rarely ($n = 4$, 19%). Furthermore, AE lesions with a solid component (type 2, 3 and 4) were significantly more frequently calcified than those with a purely cystic component (type 1 and 5, $p < 0.0001$).

The mean ADC_{total}, ADC_{min} and ADC_{max} for all AE lesions were 1.73 ± 0.50, 0.76 ± 0.38 and 2.63 ± 0.76 × 10^{-3} mm^2/s, respectively (Table 1). The mean ADC_{total} for type 1, type 2, type 3, type 4 and type 5 lesions were 1.97 ± 1.01, 1.76 ± 0.53, 1.73 ± 0.41, 1.15 ± 0.42 and 1.76 ± 0.44 × 10^{-3} mm^2/s, respectively (Fig. 4a). No significant differences in ADC_{total} were found between the five lesion types, except for type 4 ($p = 0.0363$). Furthermore, there were no significant differences in ADC_{min} and ADC_{max}, except that type 5 lesions had significantly higher ADC_{min} than all others (1.00 ± 0.36 × 10^{-3} mm^2/s, $p = 0.0003$), whereas type 4 significantly lower ADC_{max} (1.59 ± 0.42 × 10^{-3} mm^2/s, $p = 0.0137$). The mean ADC of the surrounding liver parenchyma was 1.21 ± 0.24 × 10^{-3} mm^2/s (range, 0.66–1.69 × 10^{-3} mm^2/s). The mean ADC_{total} for all AE lesions normalised with the ADC of the surrounding liver parenchyma ($ADC_{lesion\text{-}to\text{-}liver}$) was 1.43 ± 0.47 × 10^{-3} mm^2/s (range, 0.55–3.08 × 10^{-3} mm^2/s). Again, no significant differences in $ADC_{lesion\text{-}to\text{-}liver}$ were found between the five lesion types, except for type 4 ($p = 0.0415$, Fig. 4b).

We noted a statistically significant correlation between the presence of solid components in AE lesions and low ADC_{min} ($r = 0.39$, $p = 0.0016$). Moreover, there was a significant correlation between the presence of calcifications and low ADC_{min} ($r = 0.31$, $p = 0.0159$). Conversely, an inverse correlation was found between lesion relative contrast enhancement and ADC_{total} ($r = -0.34$, $p = 0.0072$). Finally, there were no significant correlations between the presence of small or large cysts and ADC_{total} ($r = 0.08$, $p = 0.5418$ and $r = 0.04$, $p = 0.7813$, respectively).

4. Discussion

AE should be diagnosed accurately and at an early stage to enable optimal patient management. If left untreated, this parasitic disease is usually fatal [1,3,4].

US and CT remain the most widely used imaging techniques for detecting AE liver lesions. While CT best depicts the characteristic calcification pattern of these lesions, the assessment of other lesion components is limited with this method [4–7].

Please cite this article in press as: Becce F, et al. Alveolar echinococcosis of the liver: Diffusion-weighted MRI findings and potential role in lesion characterisation. Eur J Radiol (2014), http://dx.doi.org/10.1016/j.ejrad.2013.12.025

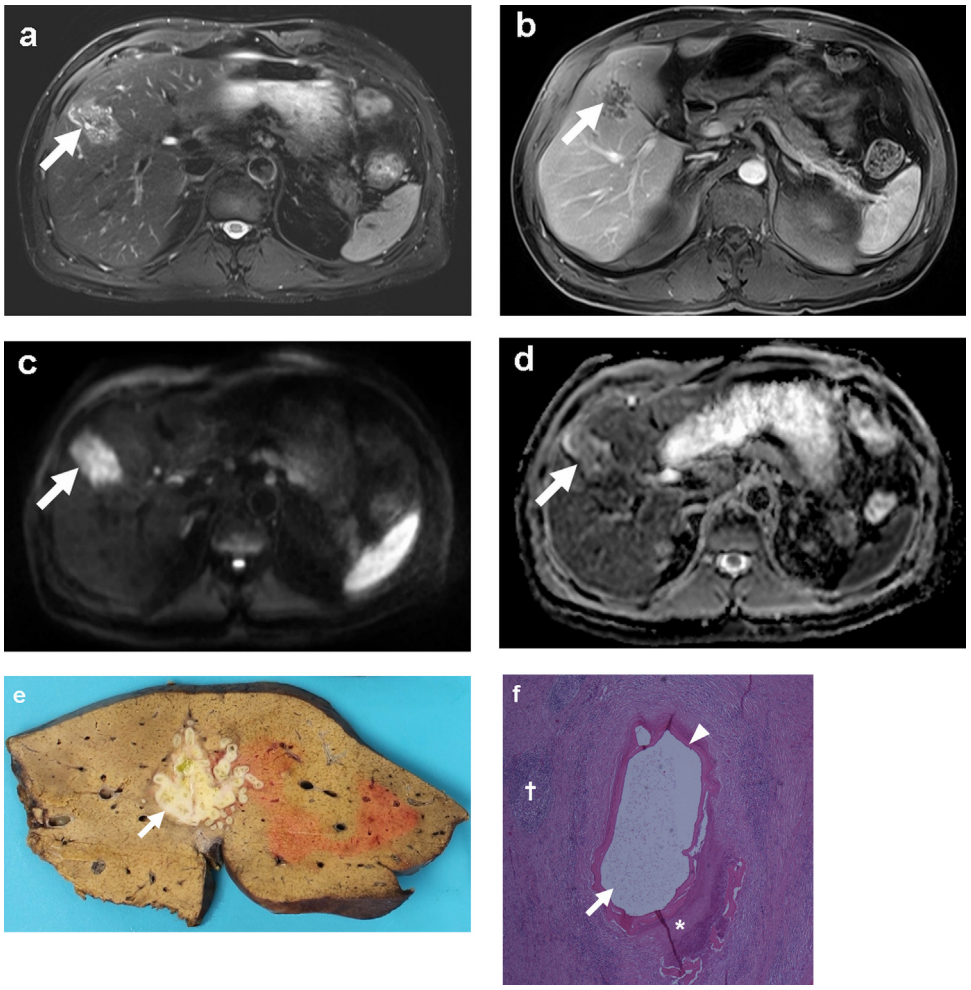

Fig. 2. 58-year-old man with liver AE. Axial FS T2-weighted (a), gadolinium-enhanced (portal venous phase) FS T1-weighted VIBE (b) and FS diffusion-weighted (*b*-value = 600 s/mm^2) SS-EPI (c) MR images, with the corresponding ADC map (d), depict a type 2 AE lesion (arrow) located in segment V. The lesion consists of multiple small round cysts with a solid component (a), and is faintly enhanced (at the periphery) after intravenous gadolinium administration (b). Relative to the surrounding liver parenchyma, the lesion remains hyperintense on the high *b*-value diffusion-weighted MR image (c), and is moderately hyperintense ($ADC_{total} = 1.61 \times 10^{-3}$ mm^2/s) on the ADC map (d). Gross pathological examination (axial section) of the partial hepatectomy specimen (e) demonstrates the characteristic alveolar (multivesicular) structure of the AE lesion. Histopathological analysis (f) reveals metacestode vesicles (arrow) with an outer acellular laminar membrane (arrowhead), surrounded by an exuberant fibroinflammatory host response (* = fibrosis, † = inflammatory cells; haematoxylin and eosin stain, original magnification 5×).

Thanks to its excellent contrast resolution, MRI is the best modality for visualising cystic and/or solid lesion components as well as the invasion of vascular, biliary, and/or extrahepatic structures [8,19,20]; MRI is therefore particularly helpful for preoperative evaluation [4,6,20]. Furthermore, Kodama's classification system was established exclusively on the various MRI patterns of AE lesions (Fig. 1) [8].

Cystic components, which consist of metacestode vesicles and liquefaction necrosis, are characterised by low signal intensity on T1-weighted and high signal intensity on T2-weighted MRI [4,8,18]. Metacestode vesicles appear as small round cysts (included in type 1, type 2, and type 3 lesions), whereas liquefaction necrosis is visualised as large and/or irregular cysts (included in type 3 and type 5 lesions). In our study, type 5 lesions (liquefaction necrosis without solid component) occurred most frequently ($n = 21$, 33%), while type 1 lesions (metacestode vesicles without solid component) were the most rare ($n = 3$, 5%). Since the purely vesicular form has been considered an initial stage of the disease [21], the small number of type 1 lesions encountered in the present investigation could mean that AE lesions progress rapidly to an advanced stage or are detected late in the disease process.

Solid components are characterised by low signal intensity on T1-weighted and low to intermediate signal intensity on T2-weighted MRI [4,8,18]. They consist of coagulation necrosis, granulomas, and/or calcifications, and reflect the chronic fibroinflammatory host response. Type 2 (metacestode vesicles with a solid component) and type 3 lesions (metacestode vesicles with a solid component surrounding liquefaction necrosis) contain variable amounts of solid components, whereas type 4 lesions consist exclusively of solid tissue [8]. In our study, type 2 lesions were the second most frequent lesion type ($n = 19$, 30%), closely followed by type 3 lesions ($n = 17$, 27%); type 4 lesions were the most rare ($n = 3$, 5%). Since type 2 and type 3 lesions together accounted for more than half of the lesions ($n = 36$, 57%), we conclude that AE liver lesions occur most often as complex lesions, thus emphasising the value of MRI in the initial evaluation. Furthermore, the fibrotic tissue in AE lesions is not always composed of well-perfused collagen, but is sometimes poorly vascularised, and may include sclerosis. Thus, no or only subtle enhancement is seen after intravenous administration of contrast medium [4–7]. However, contrast enhancement has not been included in Kodama's classification system, nor has the presence of calcifications. The latter

Please cite this article in press as: Becce F, et al. Alveolar echinococcosis of the liver: Diffusion-weighted MRI findings and potential role in lesion characterisation. Eur J Radiol (2014), http://dx.doi.org/10.1016/j.ejrad.2013.12.025

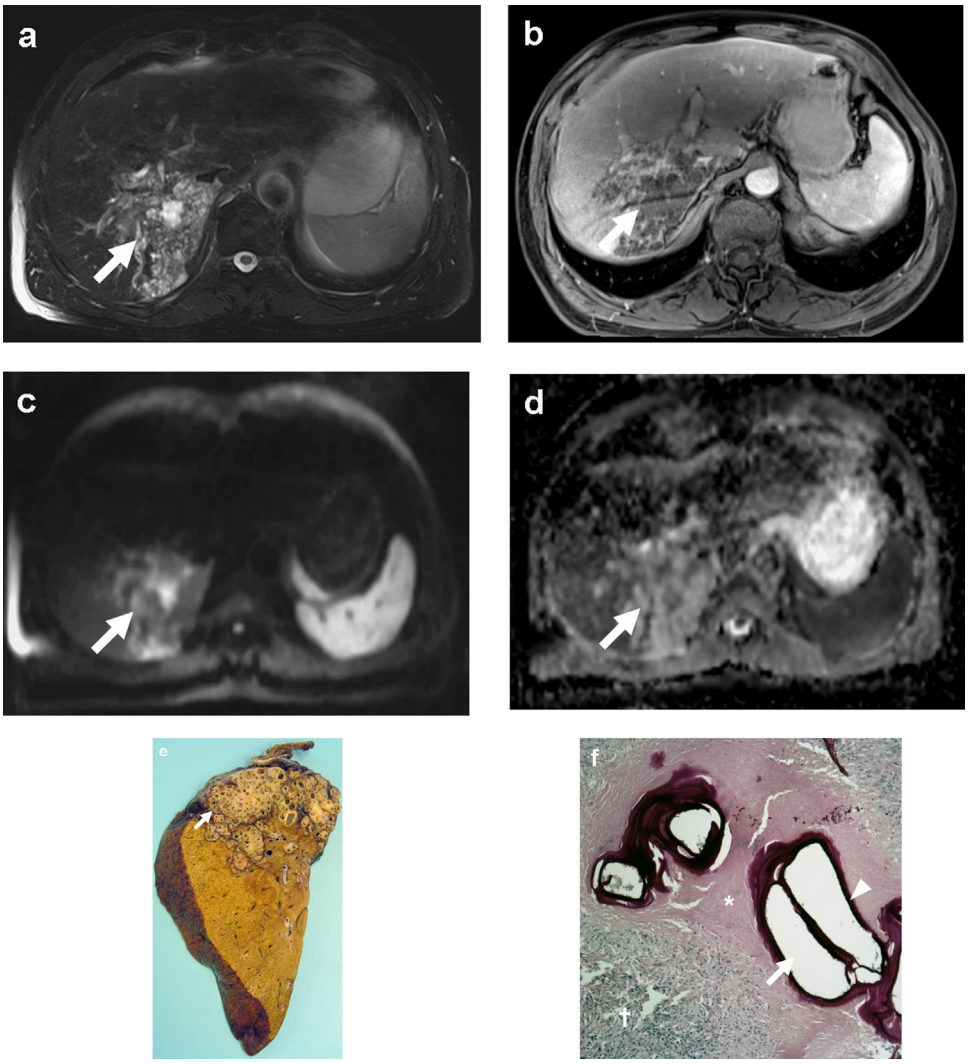

Fig. 3. 72-year-old man with liver AE. Axial FS T2-weighted (a), gadolinium-enhanced (portal venous phase) FS T1-weighted VIBE (b) and FS diffusion-weighted (*b*-value = 600 s/mm^2) SS-EPI (c) MR images, with the corresponding ADC map (d), depict a type 3 AE lesion (arrow) located in segment VII. The lesion is composed of multiple small round cysts with a solid component surrounding a large irregular cyst (a), and is faintly enhanced (at the periphery) after intravenous gadolinium administration (b). Compared to the surrounding liver parenchyma, the lesion remains hyperintense on the high *b*-value diffusion-weighted MR image (c), and is moderately hyperintense (ADC_{total} = 1.78 × 10^{-3} mm^2/s) on the ADC map (d). Gross pathological examination (sagittal section) of the partial hepatectomy specimen (e) shows the typical alveolar (multivesicular) structure of the AE lesion. Histopathological analysis (f) reveals metacestode vesicles (arrow) with an outer acellular laminar membrane (arrowhead), surrounded by an exuberant fibroinflammatory host response (* = fibrosis, † = inflammatory cells; periodic acid-schiff stain, original magnification 10×).

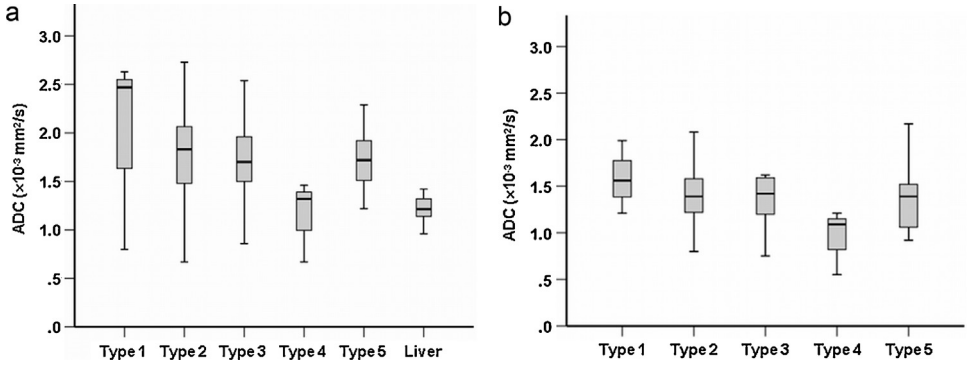

Fig. 4. Box-and-whisker diagrams illustrate the variations in ADC_{total} (a) and $ADC_{lesion\text{-}to\text{-}liver}$ (b) as a function of the AE lesion type. No statistically significant differences in ADC_{total} (p = 0.3010) and $ADC_{lesion\text{-}to\text{-}liver}$ (p = 0.2288) were found between the five lesion types, except for type 4, which had significantly lower ADC_{total} (1.15 ± 0.42 × 10^{-3} mm^2/s, p = 0.0363) and $ADC_{lesion\text{-}to\text{-}liver}$ (0.95 ± 0.35 × 10^{-3} mm^2/s, p = 0.0415) than all others.

Please cite this article in press as: Becce F, et al. Alveolar echinococcosis of the liver: Diffusion-weighted MRI findings and potential role in lesion characterisation. Eur J Radiol (2014), http://dx.doi.org/10.1016/j.ejrad.2013.12.025

Table 1
MRI (including DWI) findings for each of the five types of AE liver lesions (according to Kodama's classification system [8]).

Item	Type 1 (n = 3)	Type 2 (n = 19)	Type 3 (n = 17)	Type 4 (n = 3)	Type 5 (n = 21)	Overall (n = 63)	P-value
Diameter (cm), mean ± SD	2.2 ± 0.3	4.0 ± 3.2	6.1 ± 2.2	1.3 ± 0.1	1.3 ± 0.3	3.4 ± 2.9	<0.0001*
Distribution (segment I/left lobe/right lobe), n (%)	1 (33%)/1 (33%)/1 (33%)	1 (5%)/6 (32%)/12 (63%)	1 (6%)/5 (29%)/11 (65%)	0 (0%)/1 (33%)/2 (67%)	4 (19%)/5 (24%)/12 (57%)	7 (11%)/18 (29%)/38 (60%)	0.4951†
Relative contrast enhancement, mean ± SD	0.35 ± 0.21	0.28 ± 0.23	0.24 ± 0.24	0.28 ± 0.04	0.35 ± 0.21	0.29 ± 0.22	0.5744*
Calcifications (on CT), n (%)	2 (67)	13 (68)	15 (88)	1 (33)	4 (19)	35 (56)	0.0002†
ADC_{total} ($\times 10^{-3}$ mm^2/s), mean ± SD	1.97 ± 1.01	1.76 ± 0.53	1.73 ± 0.41	1.15 ± 0.42	1.76 ± 0.44	1.73 ± 0.50	0.3010*
ADC_{min} ($\times 10^{-3}$ mm^2/s), mean ± SD	0.61 ± 0.29	0.71 ± 0.36	0.59 ± 0.31	0.62 ± 0.44	1.00 ± 0.36	0.76 ± 0.38	0.0076*
ADC_{max} ($\times 10^{-3}$ mm^2/s), mean ± SD	2.98 ± 1.61	2.74 ± 0.75	2.87 ± 0.60	1.59 ± 0.42	2.43 ± 0.64	2.63 ± 0.76	0.0353*
ADC_{liver} ($\times 10^{-3}$ mm^2/s), mean ± SD	NA	NA	NA	NA	NA	1.21 ± 0.24	NA
$ADC_{lesion\text{-}to\text{-}liver}$ ($\times 10^{-3}$ mm^2/s), mean ± SD	1.59 ± 0.39	1.55 ± 0.57	1.47 ± 0.52	0.95 ± 0.35	1.34 ± 0.31	1.43 ± 0.47	0.2288*

ADC = apparent diffusion coefficient, AE = alveolar echinococcosis, DWI = diffusion-weighted MRI, n = number, NA = not applicable, SD = standard deviation.
* One-way analysis of variance (followed by pairwise comparisons).
† Chi-squared test.

usually correspond to a near signal void on T1- and T2-weighted MRI, and are therefore not easily detected with this technique [19,20].

Over the past few years, DWI has been increasingly used as an adjunct to abdominal MRI due to its ability to detect and characterise FLLs without the use of gadolinium-based contrast agents [10–12]. DWI exploits the microscopic random motion of water protons to measure the diffusion of fluid in tissues [9,10]. Diffusion is inversely related to cellularity, cell membrane integrity, and lipophilicity; higher tissue cellularity leads to less diffusion and, consequently, lower ADC values [22]. Conversely, in tissues with low cellularity or disrupted cell membranes, diffusion is relatively free or unimpeded. Thus, cellular or solid liver lesions (tumours, abscesses, fibrosis) are characterised by far lower ADC values than purely cystic lesions, such as simple biliary cysts [11,12]. Our results are in accordance with this principle, since type 1 lesions (metacestode vesicles) had the highest ADC_{total} ($1.97 \pm 1.01 \times 10^{-3}$ mm^2/s) of the five lesion types, followed by type 5 (liquefaction necrosis) and type 2 lesions (1.76 ± 0.44 and $1.76 \pm 0.53 \times 10^{-3}$ mm^2/s, respectively). Using a similar DWI protocol, Bruegel et al. reported an ADC value of $3.02 \pm 0.31 \times 10^{-3}$ mm^2/s for simple biliary cysts [11]. In the present study, ADC values were clearly lower for AE liver lesions, particularly for purely cystic lesions (type 1 and type 5). ADC measurements may thus help distinguish AE liver lesions from simple biliary cysts, which would be particularly helpful for type 5 lesions, as they mimic simple biliary cysts.

Several studies have reported the utility of ADC measurements in characterising FLLs [11,12,17,23–25]. In general, benign liver lesions have higher ADC values than malignant lesions, with a variable degree of overlap and ADC cutoffs ranging from 1.47×10^{-3} mm^2/s to 1.60×10^{-3} mm^2/s [11,12,17,23–25]. The ADC_{total} for each of the five AE lesion types were clearly above this range (with the exception of type 4), highlighting the utility of ADC measurements as a supplementary tool for distinguishing most AE lesions from liver malignancies, especially those that resemble AE in morphology. This is especially pertinent for cholangiocarcinoma, which is often the main differential diagnosis at the initial detection of AE [4,8,21]. A mean ADC of $1.31 \pm 0.29 \times 10^{-3}$ mm^2/s for cholangiocarcinoma was previously reported by Cui et al. [26], which is clearly lower than the ADC_{total} of all AE lesion types in the present investigation (except type 4). However, Cui et al. only included the extrahepatic type of lesion, and no results for intrahepatic cholangiocarcinoma have been published so far.

To our knowledge, the current work is the first to report the DWI findings in liver AE and investigate the usefulness of ADC values for differentiating the five types of AE lesions. ADC values were not helpful for this distinction, except for purely solid (type 4) lesions ($p = 0.0363$). This type may be easily distinguished from the other types by measuring ADC values. Furthermore, the presence of solid component within any type of AE lesion significantly correlated with a lower ADC_{min} ($r = 0.39$, $p = 0.0016$). Thus, solid content causes a greater restriction in the diffusion of water protons compared to that resulting from purely cystic AE lesions. This observation may be due to several factors. Firstly, the presence of chronic fibroinflammatory tissue has been associated with low ADC values due to its high cellularity and low proton density [10,22]. An association between low ADC values and the presence of fibroinflammatory tissue is confirmed by our observation that ADC_{total} inversely correlated with relative contrast enhancement ($r = -0.34$, $p = 0.0072$); this observation is most likely due to the accumulation of gadolinium in the underlying fibrotic component. Secondly, the presence of cellular debris within the central necrosis has also been reported to cause low ADC, primarily due to its high viscosity, as initially demonstrated in hepatic abscess cavities [10,22,27]. Thirdly, the presence of coagulation necrosis within the solid component leads

to low ADC values due to the resulting paucity of water molecules [4].

Attributing distinct ADC values to the various morphologic components of AE liver lesions may enable the detection of increased or reduced disease activity via changes in ADC values, as has been demonstrated with several hepatic and abdominal tumours [28]. Combined with MRI, we envision the use of these ADC values as a biomarker during follow-up, a radiation-free and more available alternative to F-18-fluorodeoxyglucose (FDG) positron-emission tomography (PET) [6,29].

We acknowledge the following limitations of our study. First, small numbers of type 1 ($n = 3$) and type 4 ($n = 3$) lesions were evaluated, compared with all other lesion types ($n \geq 17$). Therefore, additional, larger studies are necessary to corroborate our results. Second, ADC measurements are known to be highly variable, as they primarily depend on the *b*-values used during the acquisition of diffusion-weighted sequences. We used a DW-SS-EPI sequence and *b*-values (50, 300 and 600 s/mm^2) that were the same as those used in other studies [11,17]. Our results are therefore comparable with those of previous studies; for example, the ADC of the surrounding liver parenchyma was 1.21×10^{-3} mm^2/s, compared with 1.24×10^{-3} mm^2/s for Bruegel et al. [11]. Finally, ADC measurements are known to be subject to inter- and intraobserver variability [30], which is why we repeated all measurements three times in succession and only recorded the median values.

5. Conclusion

MRI performed with conventional sequences may not enable straightforward diagnosis of liver AE because the widely varying imaging results depend on the parasite's growth stage [4,5]. Furthermore, the infiltrative character of AE liver lesions mimics slow-growing primary or secondary liver malignancies. As demonstrated in the present investigation, ADC values are helpful for narrowing the differential diagnosis, particularly for excluding simple biliary cysts and malignant lesions. However, ADC values were not useful for distinguishing the different AE lesion types, except for one. Therefore, we recommend the routine addition of diffusion-weighted sequences when investigating liver AE, as well as the use of ADC values as a complementary tool for reaching the correct diagnosis.

Conflict of interest

The authors declare they have no conflict of interest.

Acknowledgements

The authors thank Philippe Frascarolo for his assistance with the statistical analysis and Jérémie Uldry for his computer graphics work.

References

[1] McManus DP, Zhang W, Li J, Bartley PB. Echinococcosis. Lancet 2003;362(9392):1295–304.
[2] Vuitton DA, Zhou H, Bresson-Hadni S, et al. Epidemiology of alveolar echinococcosis with particular reference to China and Europe. Parasitology 2003;127(Suppl.):S87–107.
[3] Kern P. Clinical features and treatment of alveolar echinococcosis. Curr Opin Infect Dis 2010;23(5):505–12.
[4] Kantarci M, Bayraktutan U, Karabulut N, et al. Alveolar echinococcosis: spectrum of findings at cross-sectional imaging. Radiographics 2012;32(7):2053–70.
[5] Czermak BV, Akhan O, Hiemetzberger R, et al. Echinococcosis of the liver. Abdom Imaging 2008;33(2):133–43.
[6] Bresson-Hadni S, Delabrousse E, Blagosklonov O, et al. Imaging aspects and non-surgical interventional treatment in human alveolar echinococcosis. Parasitol Int 2006;55(Suppl.):S267–72.
[7] Reuter S, Nüssle K, Kolokythas O, et al. Alveolar liver echinococcosis: a comparative study of three imaging techniques. Infection 2001;29(3):119–25.
[8] Kodama Y, Fujita N, Shimizu, et al. Alveolar echinococcosis: MR findings in the liver. Radiology 2003;228(1):172–7.
[9] Bammer R. Basic principles of diffusion-weighted imaging. Eur J Radiol 2003;45(3):169–84.
[10] Chandarana H, Taouli B. Diffusion and perfusion imaging of the liver. Eur J Radiol 2010;76(3):348–58.
[11] Bruegel M, Holzapfel K, Gaa J, et al. Characterization of focal liver lesions by ADC measurements using a respiratory triggered diffusion-weighted single-shot echo-planar MR imaging technique. Eur Radiol 2008;18(3):477–85.
[12] Gourtsoyianni S, Papanikolaou N, Yarmenitis Maris T, Karantanas A, Gourtsoyiannis N. Respiratory gated diffusion-weighted imaging of the liver: value of apparent diffusion coefficient measurements in the differentiation between most commonly encountered benign and malignant focal liver lesions. Eur Radiol 2008;18(3):486–92.
[13] Ceçe H, Gündoğan M, Karakaş O, et al. The role of diffusion-weighted magnetic resonance imaging in the classification of hepatic hydatid cysts. Eur J Radiol 2013;82(1):90–4.
[14] Inan N, Arslan A, Akansel G, et al. Diffusion-weighted imaging in the differential diagnosis of simple and hydatid cysts of the liver. AJR Am J Roentgenol 2007;189(5):1031–6.
[15] Oruç E, Yildirim N, Topal NB, Kiliçturgay S, Akgöz S, Savci G. The role of diffusion-weighted MRI in the classification of liver hydatid cysts and differentiation of simple cysts and abscesses from hydatid cysts. Diagn Interv Radiol 2010;16(4):279–87.
[16] Sonmez G, Sivrioglu AK, Mutlu H, et al. Is it possible to differentiate between hydatid and simple cysts in the liver by means of diffusion-weighted magnetic resonance imaging? Clin Imaging 2012;36(1):41–5.
[17] Holzapfel K, Bruegel M, Eiber M, et al. Characterization of small (≤10 mm) focal liver lesions: value of respiratory-triggered echo-planar diffusion-weighted MR imaging. Eur J Radiol 2010;76(1):89–95.
[18] Choji K, Fujita N, Chen M, et al. Alveolar hydatid disease of the liver: computed tomography and transabdominal ultrasound with histopathological correlation. Clin Radiol 1992;46(2):97–103.
[19] Balci NC, Tunaci A, Semelka RC, et al. Hepatic alveolar echinococcosis: MRI findings. Magn Reson Imaging 2000;18(5):537–41.
[20] Claudon M, Bessieres M, Regent D, et al. Alveolar echinococcosis of the liver: MR findings. J Comput Assist Tomogr 1990;14(4):608–14.
[21] Rubini-Campagna A, Kermarrec E, Laurent V, Régent D. Hepatic and extrahepatic alveolar echinoccosis: CT and MR imaging features. J Radiol 2008;89(6):765–74.
[22] Morani AC, Elsayes KM, Liu PS, et al. Abdominal applications of diffusion-weighted magnetic resonance imaging: where do we stand. World J Radiol 2013;5(3):68–80.
[23] Namimoto T, Yamashita Y, Sumi S, Tang Y, Takahashi M. Focal liver masses: characterization with diffusion-weighted echo-planar MR imaging. Radiology 1997;204(3):739–44.
[24] Taouli B, Vilgrain V, Dumont E, Daire JL, Fan E, Menu Y. Evaluation of liver diffusion isotropy and characterization of focal hepatic lesions with two single-shot echo-planar MR imaging sequences: prospective study in 66 patients. Radiology 2003;226(1):71–8.
[25] Parikh T, Drew SJ, Lee VS, et al. Focal liver lesion detection and characterization with diffusion-weighted MR imaging: comparison with standard breath-hold T2-weighted imaging. Radiology 2008;246(3):812–22.
[26] Cui XY, Chen HW, Cai S, et al. Diffusion-weighted MR imaging for detection of extrahepatic cholangiocarcinoma. Eur J Radiol 2012;81(11):2961–5.
[27] Chan JH, Tsui EY, Luk SH, et al. Diffusion-weighted MR imaging of the liver: distinguishing hepatic abscess from cystic or necrotic tumor. Abdom Imaging 2001;26(2):161–5.
[28] Cui Y, Zhang XP, Sun YS, Tang L, Shen L. Apparent diffusion coefficient: potential imaging biomarker for prediction and early detection of response to chemotherapy in hepatic metastases. Radiology 2008;248(3):894–900.
[29] Stumpe KD, Renner-Schneiter EC, Kuenzle AK, et al. F-18-fluorodeoxyglucose (FDG) positron-emission tomography of *Echinococcus multilocularis* liver lesions: prospective evaluation of its value for diagnosis and follow-up during benzimidazole therapy. Infection 2007;35(1):11–8.
[30] Lu TL, Meuli RA, Marques-Vidal PM, Bize P, Denys A, Schmidt S. Interobserver and intraobserver variability of the apparent diffusion coefficient in treated malignant hepatic lesions on a 3.0 T machine: measurements in the whole lesion versus in the area with the most restricted diffusion. J Magn Reson Imaging 2010;32(3):647–53.

Please cite this article in press as: Becce F, et al. Alveolar echinococcosis of the liver: Diffusion-weighted MRI findings and potential role in lesion characterisation. Eur J Radiol (2014), http://dx.doi.org/10.1016/j.ejrad.2013.12.025